Structural, electronic and magnetic investigations on PLD based $La_2Ni_{1-x}Fe_xMnO_6$ disordered thin films

Pravin M. Tirmali, Sagar M. Mane, Snehal L. Kadam, Shrinivas B. Kulkarni[*]

Department of Physics, The Institute of Science, 15 Madam Cama Rd, Mumbai, 400020, India

[*]Corresponding author: E-mail: sbk_physics@yahoo.com

Abstract

The double perovskite materials show the magnetic semiconductor, magneto-optic and magneto-capacitance like interesting properties. It is predicted that the B-site substitution in this system may results in interesting properties. $La_2Ni_{1-x}Fe_xMnO_6$ thin films are deposited on Pt/Ti/ Si(100) substrate by Pulse Laser Deposition (PLD) technique. The films were uniform, fine grain and stoichiometric deposited at very low O_2 pressure. The XRD of $La_2Ni_{1-x}Fe_xMnO_6$ thin films exhibits rhombohedral (R-3) phase. The peak broadening appears in Raman spectra at antistretching (518 cm^{-1}) and stretching (656 cm^{-1}) modes with presence of overtone modes at 1308 cm^{-1} in $La_2Ni_{1-x}Fe_xMnO_6$ thin film samples. XPS analysis reveals the presence of La^{3+}, NiO, Ni^{3+}, Fe^{3+}, Mn^{3+} and oxygen vacancies in samples. The Ni^{3+} and Mn^{3+} antiferromagnetic coupling is responsible for decrease in saturation magnetization M_s from 4.78 to 2.74 μ_B/f.u as Fe substitution increases from 0.1 to 0.3 at 5K. The increase in grain size, peak broadening and decrease in magnetization of $La_2Ni_{1-x}Fe_xMnO_6$thin film samples suggest presence of antisite defects and antisite phase boundary. The present work will helpful to study the effect of B site substitution on La_2NiMnO_6 thin films structural, electronic and magnetic properties in order to make it suitable candidate for potential applications. Copyright © 2017 VBRI Press.

Keywords: Double perovskite, PLD, raman spectra, antisite defects, antisite phase boundary.

Introduction

Double perovskites are the materials of interest in recent years. It exhibits multiferroic nature, where ferromagnetic and ferroelectric orders coexist [**1-2**]. The double perovskites have wide range of applications such as magnetodielectric capacitors [**3-4**], spin filtering tunnel junctions [**5-6**], solid-state thermoelectric Peltier coolers [**7**], solar cell application [**8**] etc. The double-perovskite structure $(A_2BB'O_6)$ is comprised of two perovskites (ABO_3) and $(AB'O_3)$. In $(A_2BB'O_6)$, A represent cations (La, Ba, Sr, Y, Ca and Ce), while B and B' are transition metal cations (Ni, Fe, Mn , Ca and Co). The different compositions of double perovskite have been explored by researchers extensively such as La_2NiMnO_6[**9-11**], Sr_2FeMoO_6[**12**], Bi_2FeCrO_6 [**13**], Y_2NiMnO_6 [**14**].

The La_2NiMnO_6 is one of interesting double perovskite material, which exhibits several properties like ferromagnetism near room temperature, dielectric properties, magnetocapacitance, magneto-resistance, ferroelectric properties [**15**], colossal magneto-dielectric and multiglass properties [**16**]. These properties of La_2NiMnO_6 are highly depends on Ni and Mn cation ordering such as Ni^{2+} and Mn^{4+} or Ni^{3+} and Mn^{3+} states. The ordered arrangement of the NiO_6 and MnO_6octahedra gives rise to 180° ferromagnetic interactions between Ni^{2+} (d^8 ,S=1) and Mn^{4+} (d^3 , S=3/2) ions governed by Kanamori-Goodenough rules [**17**]. Recent studies show the microwave sintering effect on properties of La_2NiMnO_6 [**18**], effect of A site (Ba) substitution effect on structural, magnetic and vibrational properties of La_2NiMnO_6 double perovskite [**19,20,21**], effect on electric and dielectric properties of B site (Mg) doping on La_2NiMnO_6[**22**], high transition temperature and short ferromagnetic ordering in La_2FeMnO_6 [**23**]. The substituted La_2NiMnO_6 composition properties were engineered to make it potential candidate for applications. The double perovskite material properties are highly synthesis sensitive [**33**]. Therefore numerous methods were used for preparation La_2NiMnO_6 such as solid-state reaction, sol-gel method etc. In present work hydroxide co-precipitation method with constant pH is used to synthesize Fe substituted La_2NiMnO_6 samples in order to obtain high crystallinity, nano size powder samples. Similarly, different techniques are employed for film fabrication such as chemical wet process [**24**], MBE [**25**] and Pulse Laser Deposition (PLD). Among these methods PLD is the most suitable techniques for fabrication of double perovskite thin film deposition. It offers the possibility of a high oxygen partial pressure during

growth and can produce good quality of films. The earlier studies also show the different substrates were used for double perovskite film formation such as STO, LAO and Pt/Ti/Si [**26-32**]. The substitution will interchange the ionic positions in $A_2BB'O_6$ lattice and also affect structural, electronic and magnetic properties of the parent material. It will be interesting to study the role of Fe substitution in ferromagnetic ordering of La_2NiMnO_6 and its effect on several factors viz. antisite defects and antisite phase boundary, transition temperature, structural, electronic and magnetic properties of parent material. Several studies were made on A and B site substitution of $A_2BB'O_6$, however very few reports available on B site partial substitution of La_2NiMnO_6 thin films. In addition, the magnetic properties depend on substrate and oxygen pressure which affect the Ni^{2+} and Mn^{4+} order. Therefore, the present investigations are based on partial substitution of Ni (B site) with Fein La_2NiMnO_6 double perovskite lattice. Here PLD based Fe substituted La_2NiMnO_6 i.e. $La_2Ni_{1-x}Fe_xO_6$ thin films have been deposited at low O_2 pressure on Pt/Ti/Si(100) substrate.

Experimental

Materials details

The chemicals used were AR Grade $La(NO_3)_3.6H_2O$, $Ni(NO_3)_2.6H_2O$, $Fe(NO_3)_3 .9H_2O$, $KMnO_4$, $MnCl_2$, KOH, NH_4OH Sd-fine chemicals India Ltd.

Material synthesis

The compositions are synthesized via hydroxide co-precipitation method and for this purpose KOH is used as a precipitating agent. The precipitates thus formed were washed for several times using dilute NH_4OH solution (pH~9.00). Use of dilute NH_4OH minimizes solubility of hydroxide ions in water. The precipitate then filtered and dried to form nano-crystalline powder of$La_2Ni_{1-x}Fe_xMnO_6$where x= 0 to 0.3. The powders were presintered at 600 °C for two hours in air and further grinded to fine powder. The 5% PVA were added as binder to form pellets (20 mm diameter) of fine powders of parent and Fe substituted La_2NiMnO_6. The pellets were sintered at high temperature in muffle furnace at 1200°C for 16 hours in air to form a required composition.

The sintered pellets were used as target material for preparation of $La_2Ni_{1-x}Fe_xMnO_6$ where x= 0 to 0.3, for thin films on Pt/Ti/Si(100) substrates by a KrF excimer pulsed laser deposition system with a wavelength of 248 nm. The thin films were deposited with a fixed energy density of 1.5 J/cm^2 and a repetition rate of 5 Hz at temperature 700 °C at O_2 pressure 20 mbar. The thin films were cooled down at 10 °C/min in an oxygen atmosphere to room temperature. The $La_2Ni_{1-x}Fe_xMnO_6$thin films were annealed in O_2 ambience at 750 °C for 1 hour.

Characterizations

The crystalline structure of $La_2Ni_{1-x}Fe_xMnO_6$thin films were determined by Rigaku Smart Lab High Resolution X-ray Diffraction (HRXRD). Spin phonon

coupling by Raman spectroscopy (Jobin Yvon, Raman or, HG 2S), surface analysis by X-ray photon spectroscopy Model: PHI 5000 Versa ProbeII (ULVAC—PHI, INC, Japan) monochromatic Al-Kα source (hν =1,486.6 eV), It contains a micro-focused (200μm, 50W, 15kV) a hemispherical analyzer and a multichannel detector. The vacuum in the range of $1x10^{-10}$ torr for analysis chamber during the measurements. The combination of low energy Ar+ ions and electrons were used to neutralize surface charge for all measurements. High-resolution spectra were recorded with analyzer pass energy of 58.7 eV at the step of 0.25 eV and 50 ms time per step. The Origin 8.5 peak fit pro software is used to deconvolution of Gaussian peaks for elemental analysis.

Results and discussion

The XRD pattern (**Fig. 1a)** of PLD grown $La_2Ni_{1-x}Fe_xMnO_6$ where x=0, 0.1,0.2 and 0.3 thin films were films prepared at 700 °C with O_2 pressure 20 mbar are crystalline in nature. The reflection at 23°, 32.6°, 47°, 52.6°, 58° indicates 012, 110, 024, 122, 3-14 hkl planes of $La_2Ni_{1-x}Fe_xMnO_6$ (PDF 01-072-8297) with the space group R-3. The estimated lattice parameters for R-3 are a= 5.498Aº, b= 5.498Aº, c=13.376Aº, α= 90º, β= 90º, γ=120º, cell volume V= 350Aº ^{3} and density ρ= 6.98. The substrate peaks were observed at 29° for Pt and 69º for Si for all compositions of $La_2Ni_{1-x}FexMnO_6$ thin. The $La_2Ni_{0.8}Fe_{0.2}MnO_6$sample shows better crystallinity as compare to $La_2NiFeMnO_6$, $La_2Ni_{0.9}Fe_{0.1}MnO_6$and $La_2Ni_{0.7}Fe_{0.3}MnO_6$ samples with weak reflections. The earlier reports suggest the R-3 single phase formation for La_2NiMnO_6 annealing temperature below 800°C in O_2 ambience [33].
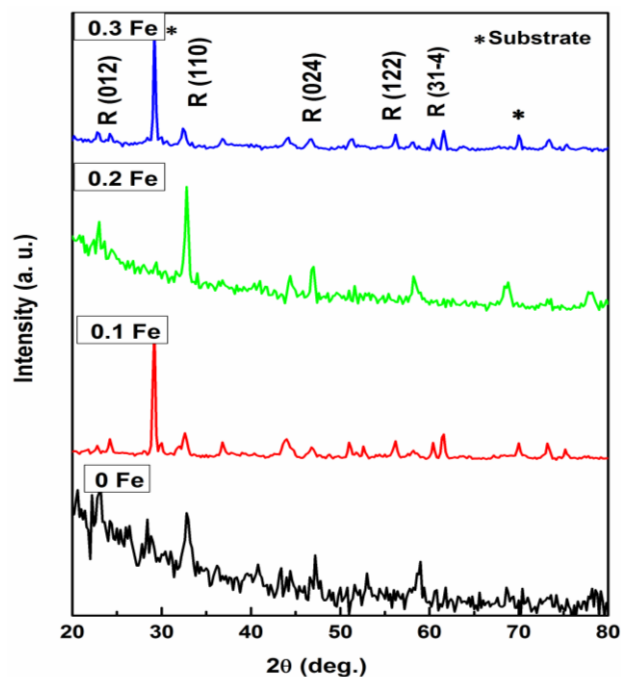

Fig. 1a. X-ray diffraction pattern of PLD grown $La_2Ni_{1-x}Fe_xMnO_6$ where x= 0, 0.1, 0.2 and 0.3 thin film samples annealed at 750°C in O_2 ambience.

The Raman spectra (**Fig. 1b**) of $La_2Ni_{1-x}Fe_xMnO_6$ PLD grown thin films samples with x = 0 to 0.3. The two well separated peaks were observed in the spectral range 518-534 cm^{-1} and 656-667 cm^{-1} for antisymmetric stretching (AS) and symmetric stretching (S) modes of vibrations respectively. For rhombohedral R-3 symmetry the possible 24 ($12A_g+12B_g$) modes are Raman active. It also exhibits additional weak and broad peaks in the spectral range1170-1308 cm^{-1} at higher frequency suggests that overtone of fundamental modes of vibrations. Here it is observed that $La_2Ni_{1-x}Fe_xMnO_6$ thin films samples exhibit shift in the peak position as well as broadening of peak as the Fe substitution increases from 0 to 0.3. The peak position shifting and broadening might be due to increasing Fe substitution at B site. It may introduce antisite defects and antisite phase boundary (APB) which leads to increase in disordering of Fe substituted La_2NiMnO_6 thin film samples. The periodic positions of Mn and Ni interchange in $A_2BB'O_6$ lattice due to Fe substitution. The above results are in good agreement with earlier reports [**20,21**]. This is further confirmed by XPS analysis which shows the presence of Fe^{3+} and Mn^{3+} states in Fe substituted samples.
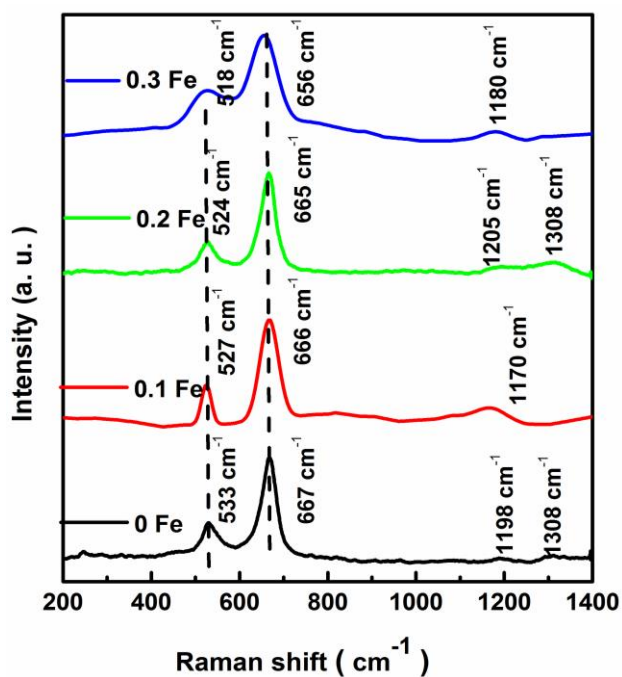
XPS spectrum of La3d (**Fig. 2a**) peaks were located at 833.38 eV / 837.6 eV (La $3d_{5/2}$) and 850.2 eV / 854.4 eV(La $3d_{3/2}$) states. It shows the mixing of La3d and Ni 2p satellite peaks in the spectrum. The spin-orbit splitting of La 3d level is 17 eV shows no chemical shift after Fe substitution in La_2NiMnO_6. The peak positions suggest the La ions present in 3^+ state. These values were observed for the double perovskites quite close to the values of pure lanthanum oxide (La_2O_3) [**34, 35**].
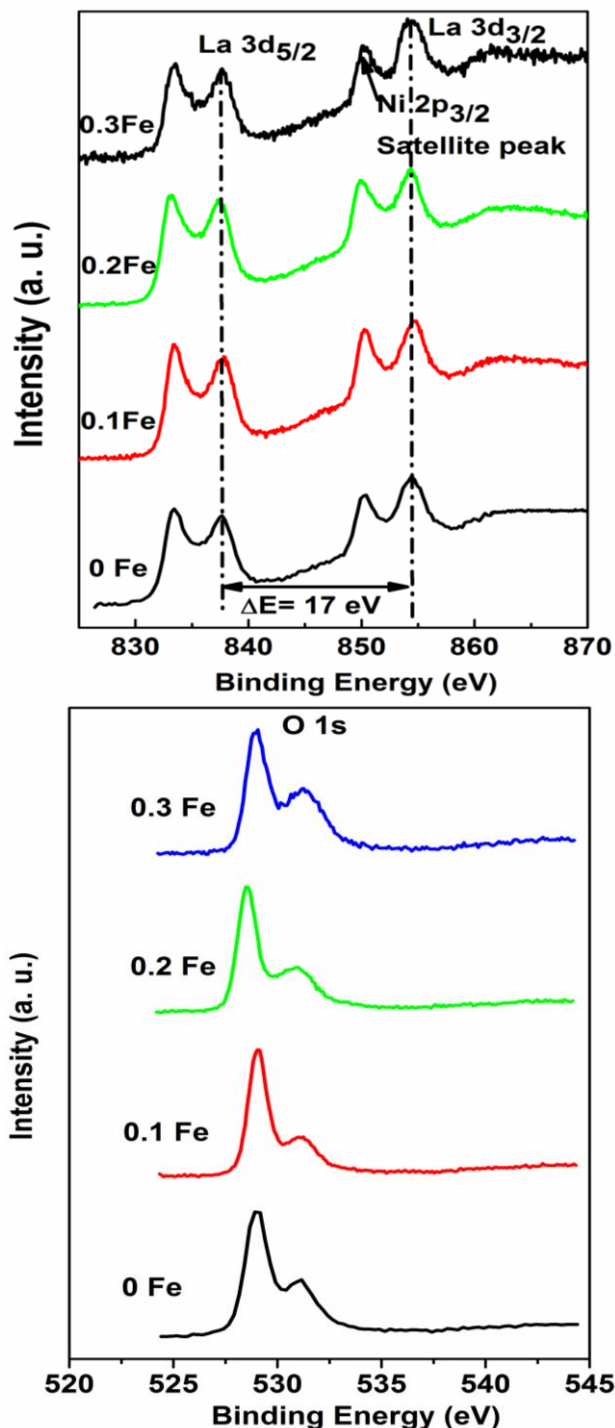

Fig. 2a. XPS spectrum of La3d and Ni 2p mixing of states with no chemical shift in $La_2Ni_{1-x}Fe_xMnO_6$ samples, **b.** XPS of O 1sfor $La_2Ni_{1-x}Fe_xMnO_6$thin film samples annealed at 750°C in O_2 ambience.

Fig. 1b. Room-temperature Raman spectra of PLD grown $La_2Ni_{1-x}Fe_xMnO_6$where x= 0, 0.1, 0.2 and 0.3, thin film samples annealed at 750°C in O_2 ambience.

The energy states of La3d, Mn2p, Ni2p, Fe2p and O1s XPS spectra of all $La_2Ni_{1-x}Fe_xMnO_6$ where x=0, 0.1, 0.2 and 0.3, thin film samples were recorded. The atomic percent of the elements were calculated from the obtained XPS data. The substitution of Fe transition metal at B site reduces the atomic % of Ni and Mn. The decrease in atomic % of Ni (B site) and Mn (B' site) may be attributed to antisite substitution of Ni and Mn ions. Fig. 2a show the XPS of La3d, Ni 2p, Mn2p, Fe 2p and O1s of the Fe substituted samples. Here we observed that the

Oxygen 1s **(Fig. 2b)** show two peaks located at 529 eV and 531.1 eV and surface absorbed O_2 ions. The O 1s shows shoulder broadening due the presence of NiO, FeOOH content in $La_2Ni_{1-x}Fe_xMnO_6$ thin film samples. The oxygen peaks shoulder broadening is increased as the Fe substitution increases it suggest increase in non-lattice oxide similar trend observed in Fe 2p spectra in $La_2Ni_{1-x}Fe_xMnO_6$ thin film samples [**41, 42**].
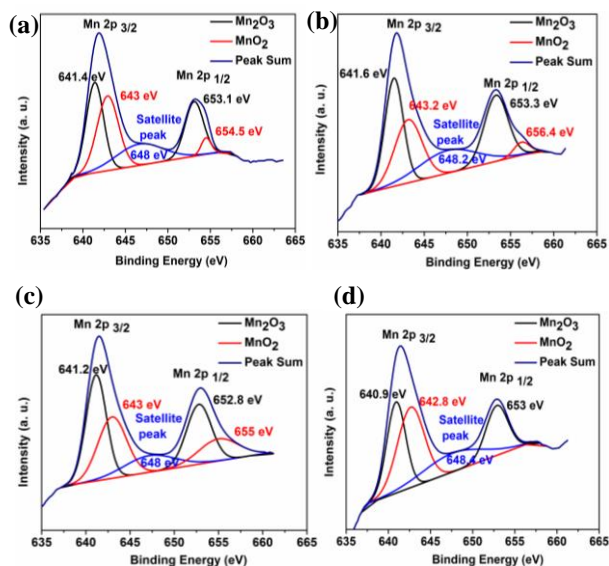

Fig. 3. XPS of Mn 2p (de-convoluted to Mn_2O_3 and MnO_2 Guassian fit) of (a) Mn2p of La_2NiMnO_6(b) Mn2p of $La_2Ni_{0.9}Fe_{0.1}MnO_6$ (c) Mn2p of $La_2Ni_{0.8}Fe_{0.2}MnO_6$ d) Mn2p of $La_2Ni_{0.7}Fe_{0.3}MnO_6$.
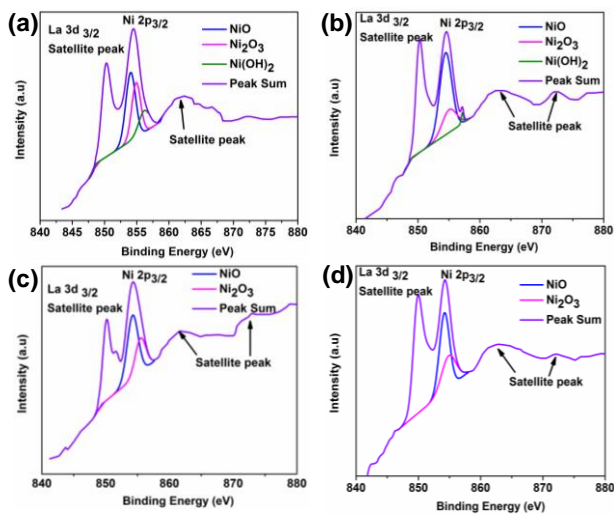

Fig. 4. XPS of mixed La3d and Ni2p peaks (deconvoluted to NiO, Ni_2O_3 and $Ni(OH)_2$) (a) Ni2p of La_2NiMnO_6(b) Ni2p of $La_2Ni_{0.9}Fe_{0.1}MnO_6$(c) Ni2p of $La_2Ni_{0.8}Fe_{0.2}MnO_6$ d) Ni2p of $La_2Ni_{0.7}Fe_{0.3}MnO_6$.

The XPS of Mn 2p **(Fig. 3(a, b, c and d))** peaks located at 642.1 eV ($Mn2p_{3/2}$) and 653.6 eV ($Mn2p_{1/2}$). The de-convolution ofthe$2p_{3/2}$and$2p_{1/2}$peaks to Gaussian fit shows the Mn_2O_3 and MnO_2 bulk are at 641.3 and 642.2 eV, respectively. The parameters are tabulated in **Table I** (supplementary data) and they show the peak shifting, Mn_2O_3 and MnO_2 peak positions. The spin orbit splitting

between asymmetric main peak $2p_{3/2}$ and $2p_{1/2}$ is nearly 11.1 eV. The peak located at 641.3 eV is assigned to Mn^{3+} ions, while the peak located at 642.2 eV is assigned to Mn^{4+} ions.The quantification of Mn 2p XPS shows higher fraction of Mn^{3+} ions as compare to Mn^{4+} ions in $La_2Ni_{1-x}Fe_xMnO_6$ samples [**36-39**].

The XPS of mixed La3d and Ni2p **(Fig. 4(a, b, c and d))** peaks located at 850.2 eV (La $3d_{3/2}$) and 654.4 eV (Ni $2p_{3/2}$) states. The de-convolution of Ni2p$_{3/2}$Gaussian peak fit shows the presence of NiO, Ni_2O_3 and $Ni(OH)_2$ peaks at 854eV, 855eV and 856.4 eV in $La_2Ni_{1-x}Fe_xMnO_6$ thin film samples. The NiO quantity decreases as the Fe substitution increases in La_2NiMnO_6 the details shown in **Table II** (supplementary data). The satellite peaks were observed at 863 eV and 872.6 eV indicates the presence of Ni^{2+} ions [**8**]. The quantification of Ni 2p spectra shows that Ni presents in high spin state and separation energy between La 3d and Ni2p is nearly 4eV.

The XPS of Fe 2p **(Fig. 5 (a, b and c))** located at 712 eV (Fe $2p_{3/2}$) and 724 eV (Fe $2p_{1/2}$) indicates the presence of Fe $^{2+}$ and Fe $^{3+}$ ions. The satellite peak situated at about 718.6 eV is a characteristic peak of Fe^{3+}. The de-convolution Fe 2p $_{3/2}$and Fe 2p $_{3/2}$ peaks shows presence FeOOH and Fe_2O_3 in$La_2Ni_{1-x}Fe_xMnO_6$. The details of Fe 2p peak shift are tabulated in **Table III** (supplementary data) for $La_2Ni_{1-x}Fe_xMnO_6$ samples. The spin orbit splitting between asymmetric main peak $2p_{3/2}$ and $2p_{1/2}$ is nearly 13 eV for Fe 2p. The position of satellite peaks and above quantification of Fe 2p clearly indicates the presence Fe $^{3+}$ ions in $La_2Ni_{1-x}Fe_xMnO_6$ thin films [**40, 41**].
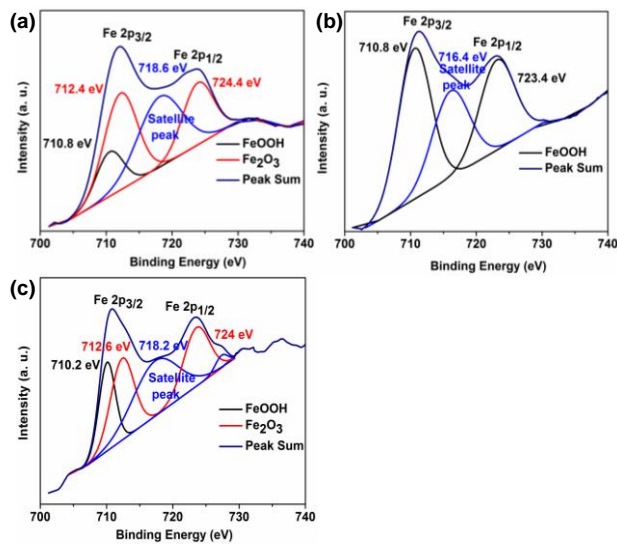

Fig. 5. XPS of Fe 2p (deconvoluted to FeOOH and Fe_2O_3) (a) Fe 2p of $La_2Ni_{0.9}Fe_{0.1}MnO_6$ (b) Fe2p of$La_2Ni_{0.8}Fe_{0.2}MnO_6$ (c)Fe2p of $La_2Ni_{0.7}Fe_{0.3}MnO_6$.

The plot of magnetic moment M as function of temperature T **(Fig. 6a)** for $La_2Ni_{1-x}Fe_xMnO_6$where x= 0, 0.1, 0.2 and 0.3 thin film samples at 1 kOe show magnetic moment decreases with increase in Fe substitution in La_2NiMnO_6 samples. It is an evidence that magnetic disordering increases in the $La_2Ni_{1-x}Fe_xMnO_6$

thin film samples as Fe substitution increases. **Table I** shows the transition temperature T_c for x= 0, 0.1, 0.2 and 0.3, $La_2Ni_{1-x}Fe_xMnO_6$ samples respectively. The higher transition temperature for $La_2Ni_{0.8}Fe_{0.2}MnO_6$ (0.2 Fe) might be due better morphology and crystalline structure as compare to x=0, 0.1 and 0.3, $La_2Ni_{1-x}Fe_xMnO_6$ samples. This decrease in magnetic moment and transition temperature will be attributed to Fe^{3+} and Mn^{3+} antiferromagnetic interactions in $La_2Ni_{1-x}Fe_xMnO_6$ thin films. It is also observed lower transition temperature in $La_2Ni_{1-x}Fe_xMnO_6$ thin films **(Fig. 6a Inset)** nearby 100K indicates presence of spin glass state and absence of ferromagnetic order at lower temperature in $La_2Ni_{1-x}Fe_xMnO_6$ thin films.
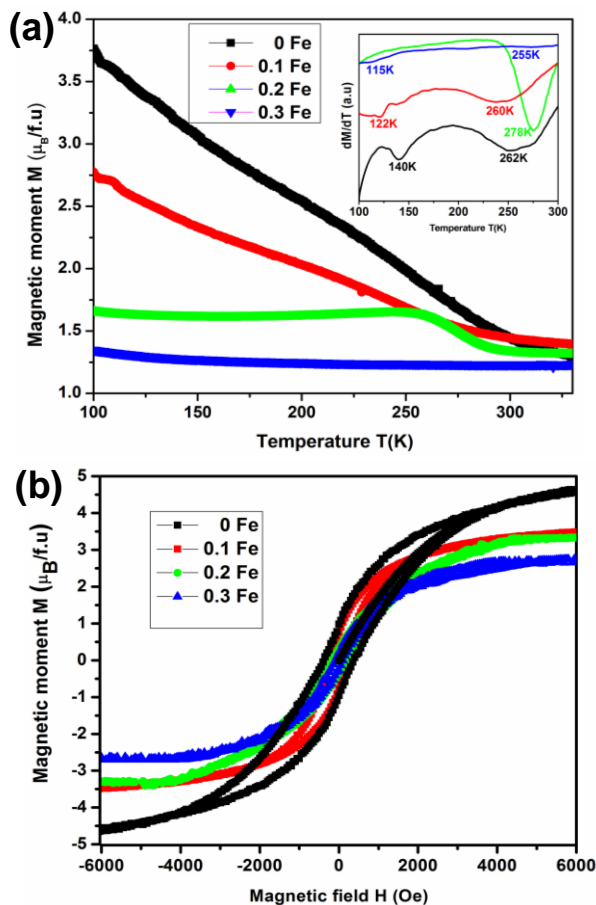
Fig 6a. Magnetic moment M as function temperature T for $La_2Ni_{1-x}Fe_xMnO_6$ PLD grown thin film samples at applied field 1000 Oe. Inset shows transition temperature of $La_2Ni_{1-x}Fe_xMnO_6$ and **(b)** magnetic hysteresis loop at temperature 5K for $La_2Ni_{1-x}Fe_xMnO_6$ PLD grown thin films.

The plot of magnetic moment (M) as function of magnetic field (H) for $La_2Ni_{1-x}Fe_xMnO_6$ thin film samples is shown in **Fig. 6b**. It shows ferromagnetic behavior of Fe substituted PLD grown thin films. **Table IV** (supplementary data) shows the coercive field H_c varies from 98 to 374 Oe, remnant magnetization varies from 0.27 to 0.95 μ_B/f.u, saturation magnetization varies from 2.74 to 4.78 μ_B/f.u for $La_2Ni_{1-x}Fe_xMnO_6$ thin film samples. The saturation magnetization for La_2NiMnO_6 sample nearly equals to theoretical value 5μ_B/f.u (spin only

moment) whereas saturation magnetization for $La_2Ni_{1-x}Fe_xMnO_6$ samples is considerably lower than 5μ_B/f.u. The significant reduction in saturation magnetization, remnant magnetization, coercive field observed as the Fe substitution level in La_2NiMnO_6 sample increases. The B site substitution results in increase in grain size, antisite defects and antisite phase boundary in Fe substituted La_2NiMnO_6.

Table I: Mn 2p spectral fitting parameters of peak position, atomic % and separation energy $La_2Ni_{1-x}Fe_xMnO_6$ thin film samples.

Sample Name	Mn_2O_3 Mn2p$_{3/2}$ Peak eV	Mn2p$_{1/2}$ Peak eV	At%	MnO_2 Mn2p$_{3/2}$ Peak eV	Mn2p$_{3/2}$ Peak eV	At%	Satellite peak eV	Separation energy eV
La_2NiMnO_6 (0 Fe)	641.3	653	59	642.9	654.4	41	646.6	11
$La_2Ni_{0.9}Fe_{0.1}MnO_6$ (0.1 Fe)	641.5	652.8	66	643.1	656.2	34	647.7	11.1
$La_2Ni_{0.8}Fe_{0.2}MnO_6$ (0.2Fe)	641.1	652.8	53	643	655	57	647.1	11.2
$La_2Ni_{0.7}Fe_{0.3}MnO_6$ (0.3 Fe)	641	652.9	64	642.7	-	36	647.6	11.3

These results are well supported by broadening of peaks and overtone modes of vibration, Oxygen vacancies, presence of NiO, Ni^{3+}/Mn^{3+} and lower transition temperature observed in M-T curve **(Fig. 6a.).** Similar kind of results was reported by Guo et. al [21] for La doped with Sr in La_2NiMnO_6 which also suggests existence of exchange bias (EB) effect in hysteresis curve, which originates from the coupling between Ni/Mn ordered FM regions and the AFM APBs derived from the antisite disorders. The earlier reports also confirm our claim presence of antisite defect and antisite phase boundary leads reduction in magnetic properties [**44,45,46**]. Kang *et al.* [**47**] reported that antisite disorder increases with La substitution with Sr and reduction in magnetization due to increase in APB. However, Wang *et al.* studied that AFM contribution or magnetization reduction is due to APB whereas antisite disorder remains unchanged for reduction in particle size. Zhou *et al.* [**48**] suggested that antisite disorder distributes over small LNMO particles.

It suggests that there could be two possible ways of reduction of saturation magnetization i) It has been observed from XPS results the presence of NiO phase which is antiferromagnetic which neglecting exchange interactions between Ni/Mn. This large volume fraction of NiO will reduce M_S by 1.5-2 μ_B/f.u [**25**]. ii) The Fe^{3+} and Mn^{3+} interaction will be more dominant as compare to Fe^{2+}-Mn^{4+} or Ni^{2+}-Mn^{4+} interaction as the Fe substitution increases in $La_2Ni_{1-x}Fe_xMnO_6$ samples. The antisite defect and antisite phase boundary leads to Jahn Teller distortions in Fe substituted $La_2Ni_{1-x}Fe_xMnO_6$ thin film samples reduce the magnetic parameters of thin films [**43**]. The comparative Table **(Table V)** of magnetic parameters of previous work and current work is provided in supporting information. It also includes various methods used for La_2NiMnO_6 synthesis and crystal phase. The comparative results show the $La_2Ni_{1-x}Fe_xMnO_6$ is monophasic and better transition temperature T_c low

saturation magnetization M_s compare to other samples except few.

Table V. Comparative table of magnetic parameters, synthesis and crystal phase of previous reports and current work on La_2NiMnO_6.

Sample Name [Ref. no.]	Synthesis Method	phase	M_s ($\mu B/f$)	T_c (K)
La_2NiMnO_6 [16]	Pechini method	P21/n	3.0	270
$La_{2-x}Sr_xNiMnO_6$ [21]	Solid-state reaction	R-3m	4.2-4.8	280
La_2NiMnO_6 [49]	Sol-gel	P21/n	6.5	275
$La_{1.9}Sr_{0.1}NiMnO_6$ [48]	Solid-state reaction	P21/n	2.2	280
La_2NiMnO_6 [30]	PLD	Pbnm	4.63	270
La_2NiMnO_6 [27]	PLD	P21/n and R-3	4.85	270 150
$(Bi_{0.9}La_{0.1})_2NiMnO_6$ [50]	PLD	-	3.5	100
La_2NiMnO_6 [51]	Solid state reaction	P21/n and R-3c	3.571	270
$La_2Ni_{1-x}Fe_xMnO_6$	Hydroxide Co-precipitation	R-3	3.53	278

Conclusion

In summary, the $La_2Ni_{1-x}Fe_xMnO_6$ thin films were epitaxialy grown on Pt/Ti/Si(100) substrate at low O_2 pressure successfully. The X-ray diffraction pattern exhibits rhombohedral (R-3) phase for all samples. The XPS analysis reveals the presence of La^{3+}, NiO, Ni^{3+}, Fe^{3+}, Mn^{3+} states and oxygen shoulder broadening in $La_2Ni_{1-x}Fe_xMnO_6$ thin film samples. The shifting and broadening of stretching and antistretching peaks in Raman spectroscopy, presence of higher fraction of NiO, Oxygen vacancies and Ni^{3+}/Fe^{3+}-Mn^{3+} interactions leads to decrease in magnetic parameters like saturation magnetization, coercivity and remnant magnetization of $La_2Ni_{1-x}Fe_xMnO_6$ thin film samples. It confirms that increase in Fe content increases disordering of La_2NiMnO_6 may results to antisite defects and antisite phase boundary i.e interchange Ni/Mn ionic positions in crystal lattice.

The lower transition temperature nearby 100 K suggests absence of ferromagnetic ordering and presence of spin glass state in Fe substituted La_2NiMnO_6 thin films. The study would helpful to understand effect of substitution, substrate and synthesis parameters on structural, electronic and magnetic ordering of La_2NiMnO_6 double perovskite.

Author's contributions

Conceived the plan: P. M. Tirmali, S. M. Mane, S. L. Kadam, S. B. Kulkarni; Performed the expeiriments: P. M. Tirmali, S. M. Mane, S. L. Kadam, S. B. Kulkarni; Data analysis: P. M. Tirmali, S. B. Kulkarni; Wrote the paper: P. M. Tirmali, S. B. Kulkarni. Authors have no competing financial interests.
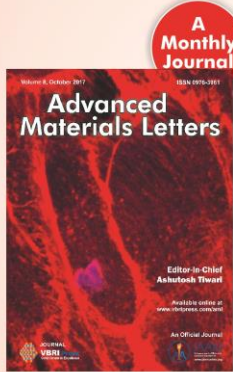
Supporting information

Supporting informations are available from VBRI Press.

References

1. Shimakawa, Y.; Azuma, M.; Ichikawa, N.; *Materials*, **2011**, *4*, 153-168.
   DOI:10.3390/ma4010153.
2. Spaldin, N. A.; Cheong, S. W.; Ramesh, R.; *Phys. Today*, **2010**,*63*, 38-43.
   DOI:http://hpc.seu.edu.cn/dong/pdf/PT63-38-2010
3. Kimura, T.; Kawamoto, S. ; Yamada, I. ; Azuma, M.; Takano, M.; Tokura, Y. ; *Phys. Rev. B*, **2003**,*67*, 180401.
   DOI:10.1103/PhysRevB.67.180401
4. Lawes, G.; Ramirez, A. P.; Varma, C. M. ; Subramanian, M. A.; *Phys. Rev. Lett.*, **2003**, *91*, 257208.
   DOI:10.1103/PhysRevLett.91.257208
5. Moodera, J. S.; Hao, X.; Gibson, G. A.; Meservey, R.; *Phys. Rev. Lett.,***1988**, *61*, 637.
   DOI: 10.1103/PhysRevLett.61.637
6. Gajek, M.; Bibes, M.; Barthelemy, A.; Bouzehouane, K.; Fusil, S.; Varela M.; Fontcuberta, J.; Fert, A.; *Phys. Rev. B* , **2005**, *72*, 020406R.
   DOI:10.1038/nmat1860
7. Fiebig, M.; Lottermoser, T.; Frohllch, D.; Goltsev, A. V. ; Pisarev, R. V.; *Nature , London*, **2002**, *419(6990)*, 818-820.
   DOI:10.1038/nature01077
8. Lan, C.; Zhao, S.; Xu, T. ; Ma, J.; Hayase, S.; Ma, T.; *J. Alloys Compd.*, **2016**, *655*, 208-214.
   DOI:10.1016/j.jallcom.2015.09.187
9. Zhang, Z. ; Jian, H.; Tang, X.; Yang, J.; Zhu X.; Sun , Y. ; *Dalton Trans.*, **2012**, *41*, 11836.
   DOI:10.1039/c2dt31214j.
10. Wu, Z. Y.; Ma, C. B.; Tang, X. G. ; Li, R.; Liu Q. X.; Chen, B. T.; Nanoscale Res. Lett., **2013**, *8*, 207.
    DOI:10.1186/1556-276X-8-207.
11. Hashisaka, M.; Kan, D.; Masuno, A.; Takano, M.; Shimakawa, Y.; Terashima, T.; Mibu, K.; *Appl. Phys. Lett.*, **2006**,*89*, 032504.
    DOI: 10.1063/1.2226997.
12. Manako, T.; Izumi, M.; Konishi, Y.; Kobayashi, K. I.; Kawasaki, M.; Tokura, Y.; *Appl. Phys. Lett.*, **1999**, *74*, 2215.
    DOI:10.1063/1.123805.
13. Nechache, R.; Harnagea, C.; Carignan, L. P.; Gautreau, O.; Pintilie, L.; Singh, M. P.; Ménard, D.; Fournier, P.; Alexe, M.; Pignolet A.; *J. Appl. Phys.,***2009**, *105*, 061621.
    DOI:10.1063/1.3073826.
14. Maiti, R. P.; Mitra, M. K.; Chakravorty, D.; *AIP Conf. Proc.*, **2013**, *1536*, 1069.
    DOI:10.1063/1.4810604.
15. Kazan, S.; Mikailzade, F. A.; Ozdemir, M.; Aktaş, B.; Rameev, B.; Intepe A.; Gupta A.; *Appl. Phys. Lett.,* **2010**, *97*, 072511.
    DOI:10.1063/1.3481678
16. Choudhury, D.; Mandal, P.; Mathieu, R.; Hazarika, A.; Rajan, S.; Sundaresan, A.; Waghmare, U. V.; Knut, R.; Karis, O.; Nordblad, P.; Sarma, D. D.; *Phys. Rev. Lett.*,**2012**,*108*, 12720.
    DOI:10.1103/PhysRevLett.108.127201.
17. Goodenough, J.; Wold, A.; Arnott, R.; Menyuk, N.; *Phys. Rev.*, **1961**,*124*, 373-384.
    DOI:10.1103/PhysRev.124.373.
18. Matli, P. R.; Mohamed A. M. A.; and Rajuru, R. R.; *Advanced Ceramic Processing*, **2015**, ISBN 978-953-51-2203-6.
    DOI:10.5772/61026
19. Barbosa, D. A. B.; Lufaso, M. W.; Reichlova , H.; Marti, X.; Rezende , M. V.S.; Maciel , A. P. ;Paschoal , C. W. A. ; *J. Alloys and Compounds*, **2016**, *663*, 899-905.
    DOI:10.1016/j.jallcom.2015.11.099
20. Tirmali, P. M.; Mane, S. M.; Patil, S. K.; Kulkarni, S. B.; *J. Mater. Sci: Mater Electron*, **2016**, *27*, 4314.

DOI:10.1007/s10854-016-4298-7.

21. Guo Y.; Shi L.; Zhou S.; Zhao J.; Wang C.; Liu W.; Wei S; J. Phys. D: Appl. Phys., **2013**, *46* , 175302.
DOI: 10.1088/0022-3727/46/17/175302

22. Cao, Z. ; Wang, L.; He, W.; Zeng, J.; Gao, Y.; Liu, J.; Leng, S.; *J. Alloys Compd.*, **2014**, *628*, 81-88.
DOI:10.1016/j.jallcom.2014.12.051

23. Jasnamol, P. P.; Lekshmi, P. N.; Thomas, S.; Suresh K. G.; Varma, M. R.; *RSC Adv.*, **2015**, *5*, 105531-105536.
DOI:10.1039/C5RA24092A.

24. Wang, T.; Fang, X.D.; Dong, W.W.; Tao, R.H.; Deng, Z.D.; Li, D.; Zhao, Y.P.; Meng, G.; Zhou, S.; Zhu, X.B.; *J. Cryst. Growth,* **2008**,*310*, 3386-3390.
DOI: 10.1016/j.jcrysgro.2008.04.028

25. Spurgeon, S. R.; Du, Y.; Droubay, T.; Devaraj, A.; Sang, X.; Longo, P.; Yan, P.; Kotula, P. G.; Shutthanandan, V.; Bowden, M. E.; LeBeau, J. M.; Wang, C. ; Sushko, P. V.; Chambers, S. A.; *Chem. Mater.*, **2016**,*28(11)* , 3814–3822.
DOI:10.1021/acs.chemmater.6b00829

26. Guo, H. Z.; Burgess, J.; Ada, E.; Street, S.; Gupta, A.; Iliev, M. N.; Kellock, A. J.; Magen, C.; Varela, M.; Pennycook, S. J.; *Phys. Rev. B: Condens. Matter Mater. Phys.,* **2008**,*77*, 174423.
DOI:10.1103/PhysRevB.77.174423

27. Singh, M. P.; Grygiel, C.; Sheets, W. C.; Boullay, P.; Hervieu, M.; Prellier, W.; Mercey, B.; Simon, C.; Raveau, B.; *Appl. Phys. Lett.*, **2007**, *91*, 012503.
DOI:10.1063/1.2753715

28. Singh, M. P.; Truong, K. D.; Jandl, S.; Fournier, P.; *Phys. Rev. B: Condens. Matter Mater. Phys.*, **2009**, *79*, 224421.
DOI:10.1103/PhysRevB.79.224421

29. Kitamura, M.; Ohkubo, I.; Kubota, M. ; Matsumoto, Y.; Koinuma, H.; Oshima, M.; *Appl. Phys., Lett.,* **2009**, *94*, 132506.
DOI:10.1063/1.3111436

30. Guo, H.; Burgess, J.; Street, S.; Gupta, A.; Calvarese, T. G.; Subramanian, M. A.; *Appl. Phys. Lett.,* **2006**, *89*, 022509.
DOI:10.1063/1.2221894

31. Tian , Y. L.; Zhang , W.; Li , L.; Lin, Y. Q.; Chen, X. M ; *J Mater Sci: Mater Electron*, **2011**, *22*,116–119.
DOI:10.1007/s10854-010-0097-8.

32. Hashisaka, M.; Kan, D.; Masuno, A.; Takano, M.; Shimakawa, Y.; *Appl. Phys. Lett.* **2006**, *89*, 032504.
DOI:10.1063/1.2226997.

33. Dass, R. I.; Yan, J. Q;. Goodenough J. B.; *Phys. Rev. B.*, **2003**, *68*, 064415.
DOI:10.1103/PhysRevB.68.064415Yi.

34. Mickevicius,S.; Grebinskij, S.; Bondarenka,V.; Vengalis, Sliuzien,B.K.; Orlowski,B.A.; Osinniy,V.; Drube,W.; *J. Alloys Compd.*, 2006, *423*, 107–111.
DOI:http://pubdb.xfel.eu/record/78577/files/OrlowskiB0702151250 1213436%5B1%5D.pdf

35. Kang, J. S.; Lee, S. M.; Kim, D. H.; Kolesnik, S.; Dabrowski, B.; Park, B.G.; Kim, J.Y.; Lee, J.; Kim, B.; Min, B. I. ; *J. Appl. Phys.,* **2010**, *107*, 09D721.
DOI:10.1063/1.3340448.

36. Wagner, C. D.; Riggs, W. M.; Davis, L. E.; Moulder, J. F.; Muilenberg, G.E.; Handbook of X-Ray Photoelectron Spectroscopy, *Perkin-Elmer,Wellesley, MA*, **1979**, 74–95.

37. Guo H. Z.; Gupta, A.; *Appl. Phys. Lett.*, **2006**, *89*, 262503.
DOI:10.1063/1.2422878

38. Carver, J. C;. Schweitzer, G. K.; Carlson, T. A.; J. Chem. Phys., **1972**, *57*, 973–981.
DOI:10.1063/1.1678348.

39. Moulder, J. F.; Stickle, W. F; Sobol, P. E.; Bomben, K. D.; Handbook of X-ray photoelectron Spectroscopy, Physical Electronics, Inc, Eden Prairie, **1995**.

40. Pham, M. H.; Dinh, C. T. ; Vuong, G. T. ; Tab, N. D.; Do, T. O.; *Phys. Chem. Chem. Phys.* **2014**, *16*, 5937.
DOI:10.1039/c3cp54629b

41. Biesinger, M. C.; Payne, B. P.; Grosvenord, A. P.; Laua, L. W. M.; Gerson, A. R.; Smart, R. St. C.; *Appl. Surf. Sci.,* **2011**, *257*, 2717–2730.
DOI:10.1016/j.apsusc.2010.10.051

42. Chen, Y. S.; Kang, J. F.; Chen, B.; Gao, B.; Liu, L. F. ; Liu, X. Y.; Wang, Y. Y.; Wu, L.; Yu, H.; Y. Wang, J. Y. Chen Q.; Wang, E. G.; *J. Phys. D: Appl. Phys.,* **2012***, 45* ,065303.
DOI:10.1088/0022-3727/45/6/065303

43. Menendez, N. G.; Sanchez, H. M.; Tornero, D.; Martínez, J. D.; Alonso, J. L.; J. A ; Chem. Mater. **2004**, *16*, 3565.
DOI:10.1021/cm049305t

44. Topwal D.; Sarma D. D.; Kato H.; Tokura Y.; and Avignon M.; Phys. Rev. B, 2006, 73, 094419.
DOI: 10.1103/PhysRevB.73.094419

45. Sarma D. D.; Sampathkumaran E. V.; Ray S.;, Nagarajan R.; Majumdar S.; Kumar Ashwani, G Nalini, TN Guru Row, Solid State Communications, 2000, 114 (9), 465-468

46. C. Meneghini, Sugata Ray, F. Liscio, F. Bardelli, S. Mobilio, and D. D. Sarma; *Phys. Rev. Lett,.***2009**, *103*, 046403.
DOI: 10.1103/PhysRevLett.103.046403

47. Kang J.S.; Lee H. J.; Kim D. H.; Kolesnik S.; Dabrowski B.; Świerczek K.; Lee J.; Kim B.; and Min B. I.; Phys. Rev. B, **2009**, *80*, 045115
DOI:10.1103/PhysRevB.80.045115

48. Zhou S. M.; Guo Y. Q.; Zhao J. Y.; Zhao S. Y.; and L. Shi, *Appl. Phy. Lett,***2010**, *96*, 262507.
DOI: 10.1063/1.3459141

49. Mao Y.; Parsons J.; McCloy J.; *Nanoscale*, **2013**, *5*, 4720
DOI: 10.1039/c3nr00825h

50.E. Langenberg; J. Rebled; S. Estrade; C. J. M. Daumont; J. Ventura; L. E. Coy; M. C. Polo; M. V. García-Cuenca; C. Ferrater,1 B. Noheda; F. Peiro; M. Varela; and J. Fontcubert; , *Phy. Rev. B*, **2012**, *86*, 085108.
DOI: 10.1103/PhysRevB.86.085108.

51. Kumar P.; Ghara, S.; Rajeswaran B; Muthu DVS. Sundaresan, A.; Sood A. K.; *Solid State Comm*., **2014**, *184*, 47-51.
DOI:10.1016/j.ssc.2014.01.002

Supporting information

Table II: Ni 2p spectral fitting parameters peak position, atomic % and separation energy of $La_2Ni_{1-x}Fe_xMnO_6$ thin film samples.

Sample Name	NiO $Ni2p_{3/2}$ Peak eV	At%	Ni_2O_3 $Ni2p_{3/2}$ Peak eV	At%	$Ni(OH)_2$ $Ni2p_{3/2}$ Peak eV	At%	Satellite peak eV	Separation energy eV
La_2NiMnO_6 (0 Fe)	853.7	67	856.1	32	-	-	-	4.2
$La_2Ni_{0.9}Fe_{0.1}MnO_6$ (0.1Fe)	854.4	74	855	24			863 873	4.3
$La_2Ni_{0.8}Fe_{0.2}MnO_6$ (0.2 Fe)	854.2	63	854.8	37	-	-	862.5 872.3	4.4
$La_2Ni_{0.7}Fe_{0.3}MnO_6$ (0.3 Fe)	853.7	75	855.6	24	857.3	0.83	861.7 871.8	4.5

Table III: Fe 2p spectral fitting parameters peak position, atomic % and separation energy of $La_2Ni_{1-x}Fe_xMnO_6$ thin film samples.

Sample Name	Fe_2O_3 $Fe2p_{3/2}$ Peak eV	$Fe2p_{1/2}$ Peak eV	At%	FeOOH $Fe2p_{3/2}$ Peak eV	$Fe2p_{1/2}$ Peak eV	At%	Satellite peak eV	Separation energy eV
$La_2Ni_{0.9}Fe_{0.1}MnO_6$ (0.1Fe)	710.8	723.9	49	712.4	-	51	718.1	13.1
$La_2Ni_{0.8}Fe_{0.2}MnO_6$ (0.2 Fe)	710.6	723.8	100	-	-	-	716.5	13.2
$La_2Ni_{0.7}Fe_{0.3}MnO_6$ (0.3 Fe)	710.1	723.4	60	712.6	-	40	717.3	13.3

Table IV: Magnetic parameters of $La_2Ni_{1-x}Fe_xMnO_6$ thin film samples.

Sample Name	Coercive field H_c (Oe)	Saturation magnetization Ms (μ_B/f.u)	Remnant Magnetization Mr (μ_B/f.u)	Transition Temperature Tc (K)
La_2NiMnO_6 (0 Fe)	374	4.78	0.95	262
$La_2Ni_{0.9}Fe_{0.1}MnO_6$ (0.1 Fe)	229.65	3.53	0.76	260
$La_2Ni_{0.8}Fe_{0.2}MnO_6$ (0.2Fe)	171.63	3.36	0.35	278
$La_2Ni_{0.7}Fe_{0.3}MnO_6$ (0.3 Fe)	98	2.75	0.27	255